Excerpt from the Proceedings of the 2011 COMSOL Conference in Stuttgart

Radiofrequency Inductively Coupled Plasmas Towards Low Pressure

Marco Cavenago*[1]
[1]INFN/LNL, Lab. Nazionali di Legnaro
*Corresponding author: v. Universitá 2, I-35020 Legnaro (PD) Italy, cavenago@lnl.infn.it

Abstract: Inductively coupled plasmas (ICP) are largely used as a convenient way to produce large ion currents in industrial applications and for particle accelerators and for the Neutral Beam Injectors (NBI) envisioned for tokamak heating (ITER project and beyond). Among specifications we have operation with gas pressure as low as possible (0.3 Pa). A multiphysics model of some major processes is here described, including a 2D axisymmetric geometry, the transferral of power from radiofrequency (rf) to electrons, the transport of density n_e and temperature T_e of these electrons and a static magnetic field B_s applied to the plasma. The ionization rate is proportional to n_e, so that a critical condition result. By averaging over a rf period, some effective plasma conductivity models can be obtained, depending from B_s and rf magnetic field strength B_f and on T_e.

Keywords: plasma, radiofrequency

1 Introduction

In radiofrequency (rf) ion sources[1, 2], electrons are subjected to static magnetic fields and to rf electric and magnetic field, with angular frequency $\omega = 2\pi f$ where f is the generator frequency. They are also subjected to collisions, with a (momentum transfer) collision frequency $\nu_c(\mathcal{E}_e)$ depending on the electron energy $\mathcal{E}_e$ and the gas density n_g. Low gas density regime is when $\omega \geq \nu_c$. We estimate $\nu_c \cong n_g v_e \sigma_c(\mathcal{E}_e)$ for some typical energy $\mathcal{E}_e$, with v_e the electron speed and σ_c the cross section. Thus

$$n_g < n_{g2} = \omega / v_e \sigma_c(\mathcal{E}_e) \qquad (1)$$

is the low gas density regime. For a Maxwellian plasma with $T_e = 4$ eV, we have a typical $E_e = 6$ eV, so that $n_{g2} = 1.3 \times 10^{20}$ m^{-3} for gas H_2, corresponding to a 0.54 Pa pressure at room temperature. Since plasma heats the gas to some extent, $p_g < 1$ Pa is a quick rule for the low pressure regime. While most industrial sources are still medium or high pressure discharge according to this rule, negative ion sources considered for NBI (aiming at 0.3) Pa operation are in the low pressure regime[3, 4].

Another low pressure regime definition is $\lambda_e > D$ where D is the source diameter (or some other typical size) and $\lambda_e(\mathcal{E}_e)$ is the electron mean free path; so $n_g \sigma_c D < 1$ is another criterion for low pressure regime (similar to previous one for $D = 0.075$ m).

Multiphysics models of inductively coupled plasma (ICP) ion sources should include n_g, T_e and n_e as variables, and thus they have to include adequate formulas for plasma conductivity in medium and low pressure regimes. Moreover, as evident from a scheme of a typical test installation[5], with approximate cylindrical symmetry (fig 1), they have to include the effect of B_f, the amplitude of the rf magnetic flux density, and of B_s the static magnetic flux density. The well known electron cyclotron resonance (ECR) is $\omega = \Omega_s$ with $\Omega_s = eB_s/m$; in our example rf frequency is 2.14 MHz, corresponding to resonance at $B_s = 0.76$ G.

Fluid models for ICP were described elsewhere[6], also at lower pressures [7, 8], assuming a given power deposition or a given conductivity. In the next section, we discuss the plasma conductivity dependence from B_s, B_f and plasma density n_e and electron temperature T_e, so that rf power deposition can be modeled with an equation for azimuthal vector potential. In the following section, the code implementation is described, with switching of complex and real solutions in a Comsol Multiphysics environment; mesh is carefully controlled, so that skin depth is everywhere resolved. Last sec-

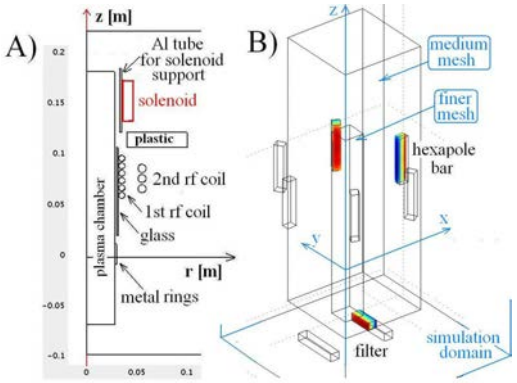

Figure 1: A) rz-plane geometry and objects for rf simulations and solenoid field; B) 3D geometry for multipole contribution to static $\mathbf{B}$; some magnets are colored

tion show some results, varying the rf coil current I_1.

2 Basic equations and assumptions

The main difficulty of rf plasma modeling is that electron plasma density n_e depends from absorbed rf power, and that absorbed rf power density p_h, among other dependencies, is proportional to n_e, which may cause a critical situation. It is common to postulate the amount of rf power absorbed into the plasma, and calculate the plasma generation and transport, which may be useful if this power could be separately measured; similarly, it can be assumed that n_e is given at some plasma position, so to calculate the plasma conductivity $\langle\sigma\rangle$ (averaged on an rf period, that is, at 1st rf harmonic) and to use this in electromagnetic calculation similar to rf oven[9]. We here will not only write equations for plasma transport and for rf, but we will also solve them selfconsistently, to obtain a really predictive model.

2.1 Single particle motion and preglow regime

At low pressure, the collision frequency $\nu_c(E_e)$ and its average ν_m on a Maxwellian EEDF (electron energy distribution function) become small, so that classical conductivity $\langle\sigma\rangle = n_e e^2/(\nu_m + i\omega)$ is unrealistically large.

Considering the friction effect of collisions, the single particle motion equation is

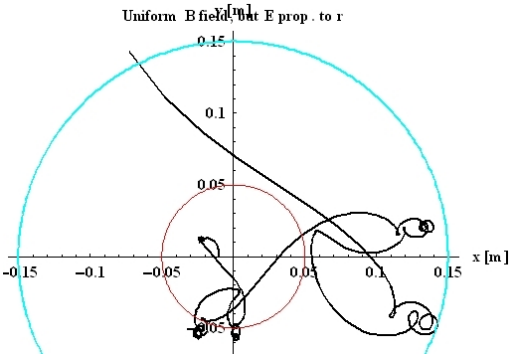

Figure 2: An electron trajectory for $\nu_c = 10^6$ Hz, $B_f = 10$ G and $B_t = -2$ G

simply written

$$m_e\dot{\mathbf{v}} = -e(\mathbf{E} + \mathbf{v}\times\mathbf{B}) - m_e\nu_c\mathbf{v} \qquad (2)$$

For example, in plasma preglow, for ideal solenoid coils, we have about

$$\begin{aligned} B_z &= B_f\,\sin(\omega t) + B_s \\ E_\vartheta &= \tfrac{1}{2}\omega\, r\, B_f \cos(\omega t) \end{aligned} \qquad (3)$$

with B_f and B_s constant and $B_x = B_y = E_r = E_z = 0$, so that motion stays in the xy plane. For some B_s and B_f, electron oscillation grows with time, as shown in fig 2; note that each time that $B_z(t)$ crosses zero, electron makes a large swing, progressively reaching larger r, where E_ϑ field is larger.

2.2 The rf coupling

Inside a rf coil, we have an oscillating current mainly azimuthal, $I_\vartheta = \Re I_1 \exp(i\omega t)$ and a driving voltage linearly rising between turns, approximately $V = \Re E_1 z \exp(i\omega t)$. As a name convention, heating due to coupling with V is called E-mode, while coupling with I_ϑ is called H-mode. Even a weak plasma shields the E-coupling; moreover, most sources include a Faraday shield in copper, so that E-mode (and ϕ) is here ignored for simplicity.

Thus the vector potential [9] is mainly azimuthal $\mathbf{A} \cong \Re(\hat{\vartheta} A_\vartheta(r,z)\mathrm{e}^{i\omega t})$. Let us take the relative permeability $\mu_r = 1$, so that A_ϑ and its derivative are continuous at material interfaces and satisfy

$$\begin{aligned} -A_{\vartheta,zz} - (A_{\vartheta,r} + r^{-1}A_\vartheta)_{,r} + \varepsilon_r q^2 A_\vartheta = \\ \mu_0 j_\vartheta = -\mu_0\sigma(i\omega A_\vartheta + r^{-1}\bar{U}_k) \end{aligned} \qquad (4)$$

where $q = \omega/c$ and ε_r is the relativity permittivity without conductivity and $\bar{U}_k$ is the

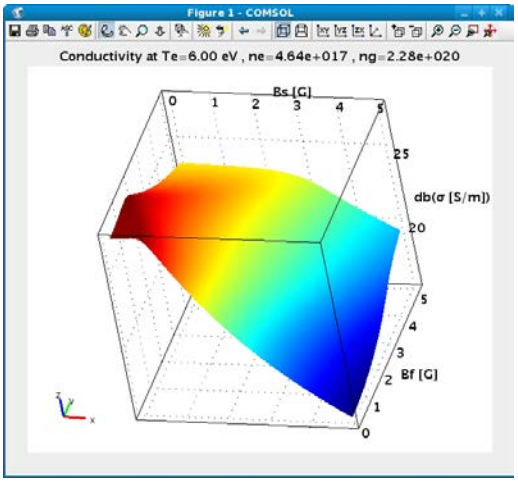

Figure 3: The conductivity vs B_s and B_f; $\mathrm{db}(\sigma)$ is $\Re 10 * log_{10}(\langle\sigma\rangle)$ averaged on a Maxwellian; $B_s = 0.76$ G is the ECR resonance

electric potential per radians applied on the k-th coil turn, $k = 1, \ldots, N$. Inside plasma we set $\sigma = \langle\sigma\rangle$, the effective plasma conductivity at the 1st rf harmonic, while inside other materials σ is the well known conductivity. We cast eq. 4 in the general PDE form

$$\operatorname{div} \mathbf{\Gamma}_u = au + \mu_0 \sigma \bar{U}_k \quad (5)$$

$$a = r^{-1} + r(i\mu_0\omega\sigma + \varepsilon_r\omega^2/c^2) \quad (6)$$

with $u = A_\vartheta$ and $\mathbf{\Gamma}_u = (ru_{,r}, ru_{,r})$. The current I_c applied to a coil is specified as input; the current $I(k) = \int_k j_\vartheta$ inside the k-turn satisfy the global equation $I(k) = I_c$. We have N such global equations, for the N unknown $\bar{U}_k$, which can be so determined.

Assuming $\omega \ll \nu_c < \Omega_f \equiv eB_f/m$ and $B_s = 0$, Ref. [1] derived the approximation

$$\langle\sigma\rangle \cong \frac{n_e e^2}{m_e\sqrt{\nu_c^2 + \Omega_f^2}}\left(1 - \frac{i\omega\nu_c}{\nu_c^2 + \Omega_f^2}\right) \quad (7)$$

To include also magnetostatic fields, a naive generalization is to substitute Ω_f with $(\Omega_f^2 + 2\Omega_s^2)^{1/2}$ in eq. 7. We here propose a more complicate formula, accounting for B_s and B_f interference[5], that is $\langle\sigma\rangle = n_e\sigma_\parallel$, with $\sigma_\parallel$ given by Eqs. 16 and 20, see Fig 3.

Versions of eqs. 7 and 20 averaged over the EEDF can be also used[10].

2.3 Plasma transport

The rate density of molecule ionization is $n_e n_g K_{iz}$, with $K_{iz}(T_e)$ a known function[11],

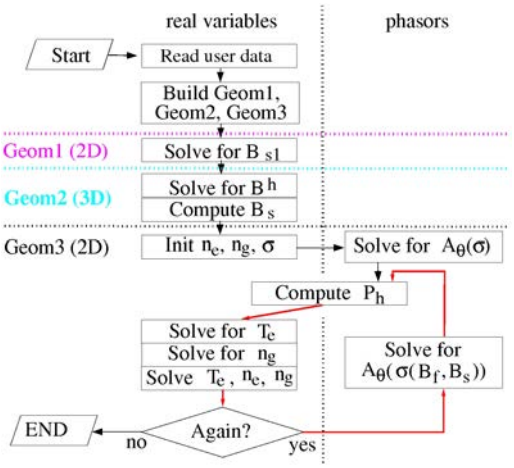

Figure 4: Scheme of script workflow

so that gas and electron balances are approximately

$$C_g(n_{g0} - n_g) = 2\pi n_g \int \mathrm{d}z\,\mathrm{d}r\, r n_e K_{iz} \quad (8)$$

$$\operatorname{div} \mathbf{\Gamma}_i = \operatorname{div} \mathbf{\Gamma}_e = n_g n_e K_{iz} \quad (9)$$

with $\mathbf{\Gamma}_e$ the flow of electrons and $\mathbf{\Gamma}_i$ the ion flow. Here n_{g0} is the gas density in a reservoir with a measuring gauge and C_g is the volume conductance between this reservoir and the plasma chamber. For plasma quasi neutrality the ambipolar equilibrium is reached, so that, including rf magnetic pressure[1]:

$$\mathbf{\Gamma}_i = -D_a(\mathbf{B}_s)\,\nabla\left(n_e + s_p\frac{B_f^2}{4\mu_0 T_e}\right) \quad (10)$$

where $s_p = 1$ and the ambipolar diffusion tensor D_a depends on magnetic field and wall kind[11]. Note that $D_a(0) = T_e/M\nu_i$, where M and ν_i are the mass and the collision frequency for ions. The ion temperature be $T_i \ll T_e$, so Bohm velocity is $u_B \cong (T_e/M)^{1/2}$. We define the ambipolar flow velocity $\mathbf{v}_a = \mathbf{\Gamma}_i/n_e$. The boundary condition which represents the sheath near a conducting wall is $\mathbf{n} \cdot \mathbf{v}_a = u_B$ with $\mathbf{n}$ the outwards normal. Insulating walls are not yet included in the model. Ion collision frequency may be estimated by $\nu_i = [(T_i/T_e)u_B^2 + v_a^2]^{1/2}/\lambda_i$, where the mean free path λ_i is approximately constant[1, 11].

The (electron) energy balance equation is

$$-\operatorname{div}(K_e \operatorname{grad} T_e) = p_h - n_e n_g K_{iz}\mathcal{E}_{iz} \quad (11)$$

where K_e is the electron thermal conductivity, $p_h = \frac{1}{2}\Re(j_\vartheta^* E_\vartheta)$ is the rf heating and $\mathcal{E}_{iz}$ is the energy spent by electrons per each

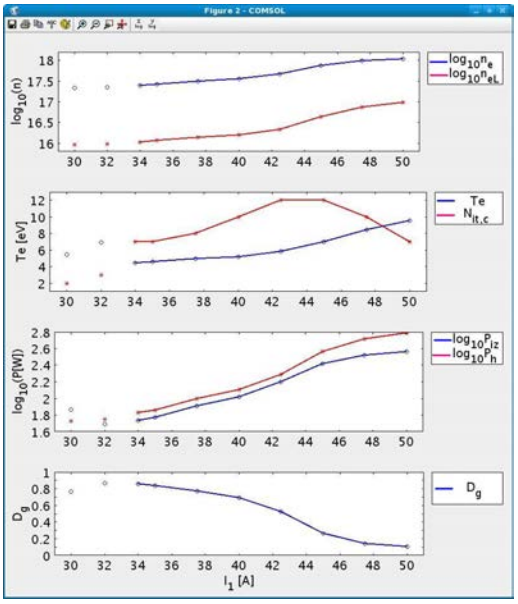

Figure 5: Summary of simulations with $p_0 = 4$ Pa and solenoid off

ionization achieved[11]; P_h is the integral of p_h over the plasma, while P_{iz} is the integral of the ionization work.

3 Implementation

The whole model is implemented in a Comsol Multiphysics environment[12], using the scripting language to translate the user input (strongly structured and contained in one text file, except for the atomic data files) into the actual geometries, and to control the flow of the solver routines. Needless to say, code is formed by a main script (temporarily called 'rf2met0main'), which calls other script and functions, and returns a 'xfem' multiphysics object and some auxiliary results (plasma conductivity tables, rf power deposition etc), which can be easily displayed and tested in the Comsol Multiphysics GUI.

The multiphysics model used is based on 3 geometries, see fig 4; geometry 1 with coordinates rz contains the solenoid, which has a clear cylindrical symmetry; let $\mathbf{B}_{s1}$ be its flux density. Geometry 3 (always referring to rz coordinates) contains the rf coil sections (whose approximate cylindrical symmetry was previously discussed) and the plasma (whose modeling in 3D can be attempted in our opinion only after 2D models work). The two geometries have different

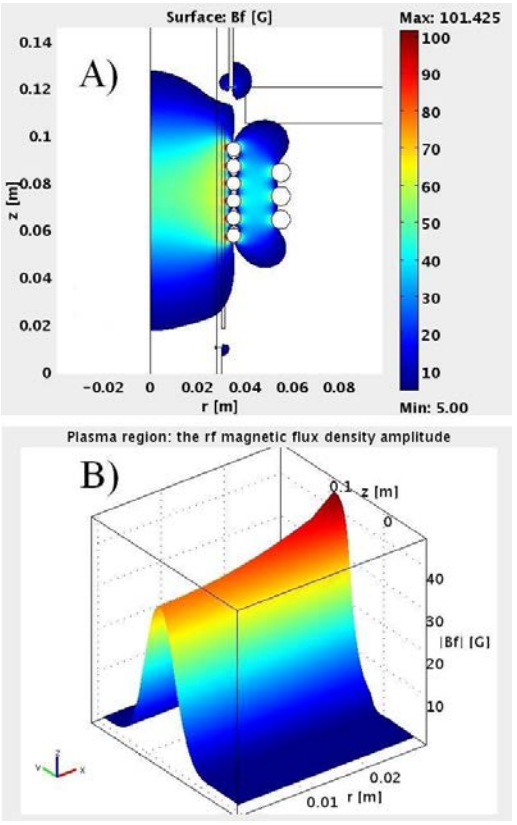

Figure 6: A) surface map of B_f, with its maxima on coil wire surfaces; B) elevation plot of B_f restricted to plasma.

meshes, in particular the mesh for rf is extremely fine inside the skin layer of conductors. Anyway the main reason to separate geometry 1 and 3 is historical, since the latter evolves from our 2008 script 'rftest12', see fig 5 in Ref. [13]. Similarly, geometry 2 (which is 3D) evolves from the script 'nbi2perm' to compute complicate multipole arrays of permanent magnets, see fig 4 in Ref. [13].

Major improvements of 'rf2met0main' over 'rftest12' are: 1) the possibility of using a parametric geometry as in 'nbi2perm' (for example, the number N of turns in a coil is a parameter) while in 'rftest12' a fixed number of turns was used (typically five); parametrization techniques was discussed elsewhere [14]; 2) eq. 20 can be used for the conductivity, while 'rftest12' had only eq. 7 and constant $\langle\sigma\rangle$ as options; 3) solenoid and hexapole fields are not read from files, but are computed in the initialization phase, so that changes of geometry are easily applied. Some minor drawbacks follow from these features, like the large program-

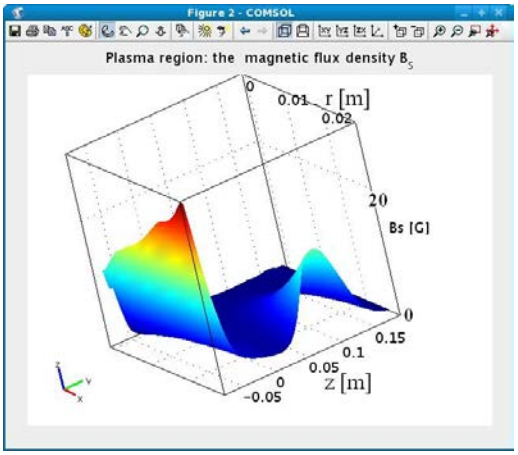

Figure 7: Elevation plot of B_s in plasma.

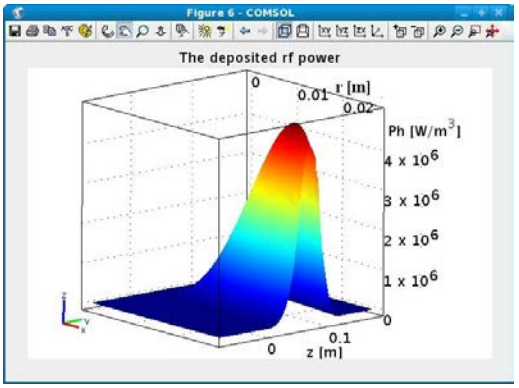

Figure 8: Elevation plot of ohmic heating P_h.

ming effort needed for '1' and the waste of few minutes of CPU time for each run due to feature '3'.

The initialization phase, as shown in fig 4, includes several steps and the approximation which projects the 3D hexapole field $\mathbf{B}^h$ onto the geometry 3 and combines it to the solenoid field $\mathbf{B}_{s1}$. For use in conductivity formula eq. 20 and similar, we define

$$B_s = (|B_{s1}|^2 + \langle {B_r^h}^2 + {B_z^h}^2 \rangle)^{1/2} \qquad (12)$$

guessing that B_ϑ^h has no effect on rf conductivity, since it is parallel to E_ϑ; here $\langle . \rangle$ is the average on ϑ; in other words the total static field squared is $B_t^2 = B_s^2 + \langle B_\vartheta^2 \rangle$. Last task in the initialization is to set $n_g = n_{g0}$ and n_e to a parabolic profile and $\langle \sigma \rangle$ to a constant, so that a first estimate of $u = A_\vartheta$ can be computed.

Iteration cycle (red arrows in fig 4) should be carefully planned, and may include redundant calculations, with the primary goal to avoid locking to wrong fixed points (in any of its steps). In each iteration, we move data between the phasor (complex) variables (A_ϑ and the $\bar{U}_k$) and the real variables (n_e, T_e and n_g); in many attempts to solve for all variables together, the real variables acquired an imaginary part, which is unacceptable. We thus keep two multiphysics objects, 'rfem' real and 'xfem' complex. First data transfer is to calculate $p_h = \frac{1}{2}\Re(j_\vartheta^* E_\vartheta)$ on a rectangular grid, and define an interpolation function representing p_h in eq. 11. We find convenient to solve first for T_e alone, with old n_e and n_g; moreover, initial guess for T_e is obtained by solving eq 11 with the LHS set to zero. Then eq. 8 for n_g is solved. Finally the system of eqs. 8-11 for n_e, T_e and n_g are solved together; due to the noise in p_h and the criticality with respect to n_e, this step is the step more likely not to converge.

After this step, we can compute $\langle \sigma \rangle$ on a grid, in the T_e, B_f and B_s space, and transfer this information by representing $\langle \sigma \rangle$ by an interpolation function in eq. 5, with $B_f = (|B_r|^2 + |B_z|^2)^{1/2}$ depending from the rf magnetic flux density. Next step is to solve eq. 5, which is nonlinear, since $\langle \sigma \rangle$ depends on B_f, as evidenced also in fig 4; anyway two internal iterations of the nonlinear solver 'femstatic' suffice to converge to a new A_ϑ solution in our test case (reason may depend from the small size of the plasma). This concludes one iteration cycle.

In the preliminary tests of this implementation, we fixed a fairly large number of iteration cycles $N_i = 14$ per run and selected runs which well converge. Typical run time is 0.25 hours on a 8 core 3 GHz Xeon workstation. In Fig. 5 the number $N_{\mathrm{it,c}}$ of cycles such that P_{iz} result is within 1% of final result is shown; $N_{\mathrm{it,c}} < 5$ means that iteration progress stopped at some phase, while $N_{\mathrm{it,c}} \geq N_i - 1$ means convergence was not jet reached; otherwise convergence is good; this is marked by joining result points with solid lines in Fig. 5).

The quantity I_1, current flowing into the 1st coil, and n_{g0} can be fairly easily measured in our installation, so that they were taken as main input in simulations. Current I_1 is measured by a Rogowski coil, and intense plasma switching on appears about at 45 A. Operating pressures p_0 between 0.5 and 10 Pa of air were observed, as measured by a Pirani gauge. Some bistabilities of

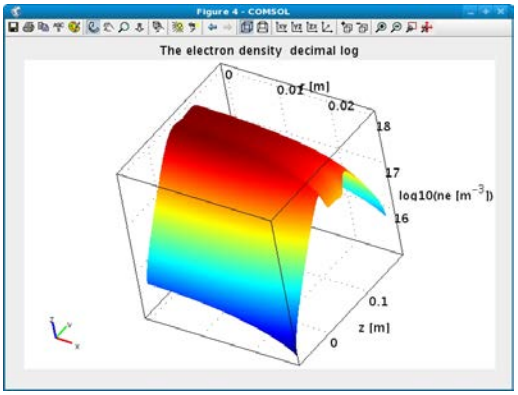

Figure 9: Elevation plot of $L_{ne} = \log_{10}(n_e/n_1)$ with $n_1 = 1\text{m}^{-3}$.

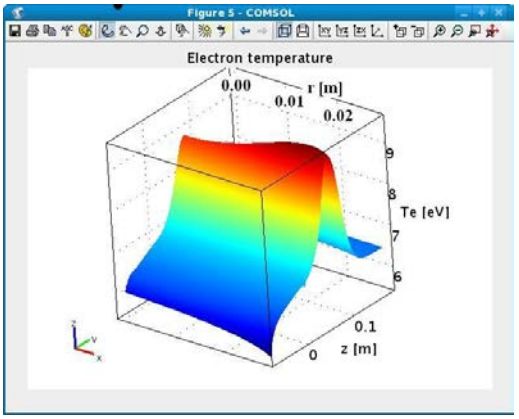

Figure 10: Elevation plot of T_e.

experimental plasmas are evident.

Only simulation results with $s_p = 0.5$ and $C_g = 0.1$ m^3/s are here discussed.

4 Results

A first set of simulations with I_1 up to 50 A and $p_0 = 4$ Pa was performed; as in real experiment $\omega/2\pi = 2.14$ MHz; results shows a strong gas depletion $D_g \equiv n_g/n_{g0} \ll 1$ and transition to a stronger plasma with $I_1 > 45$ A (see Fig 5). Convergence with $s_p = \frac{1}{2}$ is now possible, thanks to smoothing of the ponderomotive term, from $I_1 = 34$ A to $I_1 = 50$ A and more.

For the $I_1 = 50$ A case, we show results in Figs. 6-10. The propagation of rf even to the plasma center is apparent in fig 6; note also some rf near the shielding rings as expected. As regards to the static field B_s we note that the averaged hexapole effect well superpose spatially to rf field, while the (averaged) filter is only visible at lower base of plasma simulation domain, see Fig. 7; B_s is rather small (below 15 G except for filter region), so that the assumption $D_a \cong D_a(0)$ is fairly justified.

The power deposition p_h peaks at some distance from the coil, see fig 8, since electron density is depleted by ponderomotive force near the coil, see fig 9. The temperature T_e peak is near the p_h peak, but T_e gently diffuses to axis; the filter produces a steep reduction of T_e, see Fig 10.

In Fig 9 we also note two maxima in $n_e(0, z)$, which means that n_e depletion due to ponderomotive force propagates even up to the axis in this small source. The ion generation increases (rapidly) with T_e and linearly with n_e, so that n_e exponentially decays moving away from the higher T_e regions. These structures are maintained also for lower I_1.

In summary a 2D model of ICP is able to capture many interesting features of plasma heating. Preliminary experimental evidences support this model, and a more systematic campaign is being prepared. The concept of ambipolar flow helped to simplify ion and electron flows and greatly simplified plasma boundary sheath, but should be improved to included drift motion[11]. All these simplications will be also necessary in a 3D model.

References

[1] M. Tuszewski, Phys. Plasmas **5** , 1198 (1998)

[2] J T Gudmundsson and M A Lieberman, Plasma Sources Sci. Technol. **6**, 540 (1997)

[3] T. Inoue et al., "Design of neutral beam system for ITER-FEAT", Fus. Eng. and Design 56-57 (2001) 517-521

[4] H. P. L. de Esch, R. S. Hemsworth, and P. Massmann, SINGAP: The European concept for negative ion acceleration in the ITER neutral injectors, Rev. Sci. Instrum., **73**, pp1045-1047 (2002)

[5] M. Cavenago and S. Petrenko, submitted to Rev. Sci: Instrum, 2011

[6] J. Brcka, Modeling Remote H2 Plasma in Semiconductor Processing Tool, Com-

sol User Conf. 2006 Boston, Proceedings (CDROM and online).

[7] Ts. Paunska, A. Shivarova, Kh. Tarnev, and Ts. Tsankov, Phys. Plasma, **18**, 023503 (2011)

[8] O. Geoffroy, H. Rouch, 3D Electromagnetic Simulation for Microwave Plasma Coupling, Comsol User Conf. Grenoble 2007, CD-ROM

[9] M.Cavenago, T. Kulevoy, and S. Petrenko, *Rev. Sci. Instrum.*, **73**, 552 (2002)

[10] G. G. Lister, Y.-M. Li, and V. A. Godyak, *J. Appl. Phys.*, **79**, 8993 (1996)

[11] M. A. Lieberman and A. J. Lichtenberg, *Principles of Plasma Discharges and Material Processing*, John Wiley, New York, 1994

[12] *Comsol Multiphysics 3.3a*, (2007), see http://www.comsol.eu

[13] M. Cavenago, T. Kulevoy, S. Petrenko, V. Antoni, M. Bigi, E. Gazza, M. Recchia, G. Serianni, P. Veltri, Rev. Sci. Instrum. 81, 02A713 (2010)

[14] M. Cavenago, R. Cavazzana, A. Masiello, N. Pilan and G. Serianni, Modeling and Optimization of Large Size Ion Beam Deflectors, Comsol User Conf. Grenoble 2007, CD-ROM

Appendix: effective electron conductivity

Combining cartesian coordinates x, y into a complex variable $x_c = x + iy$ (and $v_c = v_x + iv_y$ and $E_c = E_x + iE_y$), we have

$$E_c = A_c \cos\psi \quad , \quad A_c = -i\tfrac{1}{2} B_f \omega x_c \quad (13)$$

where A_c is the local amplitude of E_c and $\psi = \omega t$ is a shorthand. Substituting in eq. 2 we get

$$\ddot{x}_c + [c_0 + 2ic_1 \sin\psi]\dot{x}_c + i\omega c_1 x_c \cos\psi = 0 \quad (14)$$

with shorthands $c_0 = \nu_c - ieB_s/m$ and $c_1 = -eB_f/2m$. As well known for Hill's equation, solution is the quasiperiodic function

$$x_c = \sum_{n=-\infty}^{n=\infty} x_n \exp t(s + in\omega) \quad (15)$$

where s is the growth rate. Let us define $q_n = x_n/x_{n-1}$ for $n > 0$ and $p_{-n} = x_n/x_{n+1}$ for $n < 0$. Substituting eq. 15 into eq. 14, we get some recurrence relations, which shows that p_n and q_n are $O(n^{-1})$; we also get a quadratic equation for s and we choose its more rapidly growing solution. We numerically verify that $|s| \ll \omega$ and that $p_1 \cong c_1 f(-\omega)$ and $q_1 \cong -c_1 f(\omega)$ with

$$f(\omega) = \frac{5}{4c_0 - i2\omega + 3\sqrt{4(c_0 + 2i\omega)^2 + 15c_1^2}} \quad (16)$$

Each electron makes a current

$$I_1 = -e\dot{x}_c = I^g \cos\psi + I^u \sin\psi + I^h \quad (17)$$

where I^g is the current in phase with E_c, I^g is the current in quadrature and I^h higher harmonics. We define the conductivity in phase $\sigma^g = I^g/A_c$ and the conductivity in time quadrature $\sigma^u = I^u/A_c$; using eq. 15

$$\sigma^g = \frac{e^2}{m}\frac{x_{-1} - x_1}{c_1 x_0} = \frac{e^2}{m}[f(-\omega) + f(\omega)] \quad (18)$$

since $x_1/x_0 = q_1$ is given by 16. Similarly

$$\sigma^u = \frac{e^2}{m}\frac{x_{-1} + x_1}{ic_1 x_0} = \frac{e^2}{im}[f(-\omega) - f(\omega)] \quad (19)$$

Conductivity is a tensor; but we consider here the conductivity parallel to the electric field, with a component in phase $\sigma^g_\parallel = \Re\sigma^g$ and one in time quadrature $\sigma^u_\parallel = \Re\sigma^u$. Passing to phasor notation

$$\sigma_\parallel = \sigma^g_\parallel + i\sigma^u_\parallel = \frac{e^2}{m}[f(-\omega) + f(\omega)^*] \quad (20)$$